tron yields were also measured. The principal contributions to the calculated yields are wide-angle pair production directly at an angle θ,[7] and small-angle pair production followed by scattering to an angle θ.[8] For the 0.5-inch Be target the former contributes about half as much as the latter. The observed yields at 1° were always significantly smaller than calculated and they increased too slowly with target thickness; at larger angles for the 0.5-inch target, the yield became increasingly greater than calculated. However, since the pion data satisfactorily met all tests and checks and since great care was not taken to obtain the correct electron yields but instead to provide electron rejection, we believe the pion yields support a large one-pion exchange contribution to high-energy pion photoproduction.

The motivation for making these pion measurements arose in discussions with Professor K. Crowe. We would like to thank the staff of the Harvard cyclotron for their aid in building and setting up the apparatus. We thank the staff of the Cambridge Electron Accelerator for their many services and their patience during the difficult days of the first experiments on a new accelerator. We wish to thank Paul F. Cooper, Jr., for general aid and advice, Dr. H. Butler for doing the magnet calculations, Dr. M. Thiebaux for various yield calculations, Dr. R. A. Schluter and Mr. A. Tamosaitis of Argonne National Laboratory for the use of a differential Cherenkov counter, and Professor S. D. Drell and Professor S. M. Berman for several illuminating discussions of the theory.

---

*This work was supported in part through funds provided by the U. S. Atomic Energy Commission.

[1]S. D. Drell, Phys. Rev. Letters 5, 278 (1960).

[2]S. D. Drell, Rev. Mod. Phys. 33, 458 (1961).

[3]For a general review of the peripheral model, see E. Ferrari and F. Selleri, Nuovo Cimento, Suppl. 24, 453 (1962).

[4]An earlier measurement of the pion photoproduction near the forward direction is reported in J. R. Kilner, R. E. Diebold, and R. L. Walker, Phys. Rev. Letters 5, 518 (1960).

[5]The data for the pion-beryllium scattering cross section were taken from the following sources: C. Chedester, P. Isaacs, A. Sachs, and J. Steinberger, Phys. Rev. 82, 958 (1951); J. W. Cronin, R. Cool, and A. Abashian, Phys. Rev. 107, 1121 (1957); A. E. Ignatenko, in CERN Symposium on High-Energy Accelerators and Pion Physics, Geneva, 1956 (CERN Scientific Information Service, Geneva, Switzerland, 1956), p. 313; M. J. Longo and B. J. Moyer, Phys. Rev. 125, 701 (1962); D. H. Stork, Phys. Rev. 93, 868 (1954); F. H. Tenney and J. Tinlot, Phys. Rev. 92, 974 (1953).

[6]R. M. Sternheimer, Phys. Rev. 101, 384 (1956).

[7]P. V. C. Hough, Phys. Rev. 74, 80 (1948).

[8]See, for example, R. Hofstadter, Ann. Rev. Nucl. Sci. 7, 272 (1957).

ELASTIC p-p CROSS SECTIONS AT HIGH MOMENTUM TRANSFERS*

G. Cocconi,† V. T. Cocconi,† A. D. Krisch, J. Orear, R. Rubinstein, and D. B. Scarl
Laboratory of Nuclear Studies, Cornell University, Ithaca, New York

and

W. F. Baker, E. W. Jenkins, and A. L. Read
Brookhaven National Laboratory, Upton, New York

(Received 11 November 1963)

A series of measurements of p-p elastic scattering at high energies and large angles has been made at the Brookhaven Alternating Gradient Synchrotron (AGS). Eighteen differential cross sections have been measured in the energy region $T_{lab} = 10$ to 30 BeV and momentum transfer region $-t = 2.3$ to 19.6 (BeV/c)^2, where $-t = q^2$ is the invariant four-momentum transfer squared. In units of inverse fermi squared, our highest value of $-t$ is 505 F^{-2}, which is about a factor of four higher than previously measured values of t. In units of reciprocal square-root inverse fermi squared, this is 0.044 or an interaction distance of $\hbar/q = 4.4\times10^{-15}$ cm. These new results show several striking features: (1) The energy dependence or "shrinkage" at constant momentum transfer becomes more pronounced the higher the momentum transfer; (2) with increasing momentum transfer the cross sections decrease less rapidly than would be expected from the trend of the previous data taken at lower momentum transfer[1]; and (3) the shapes of the observed

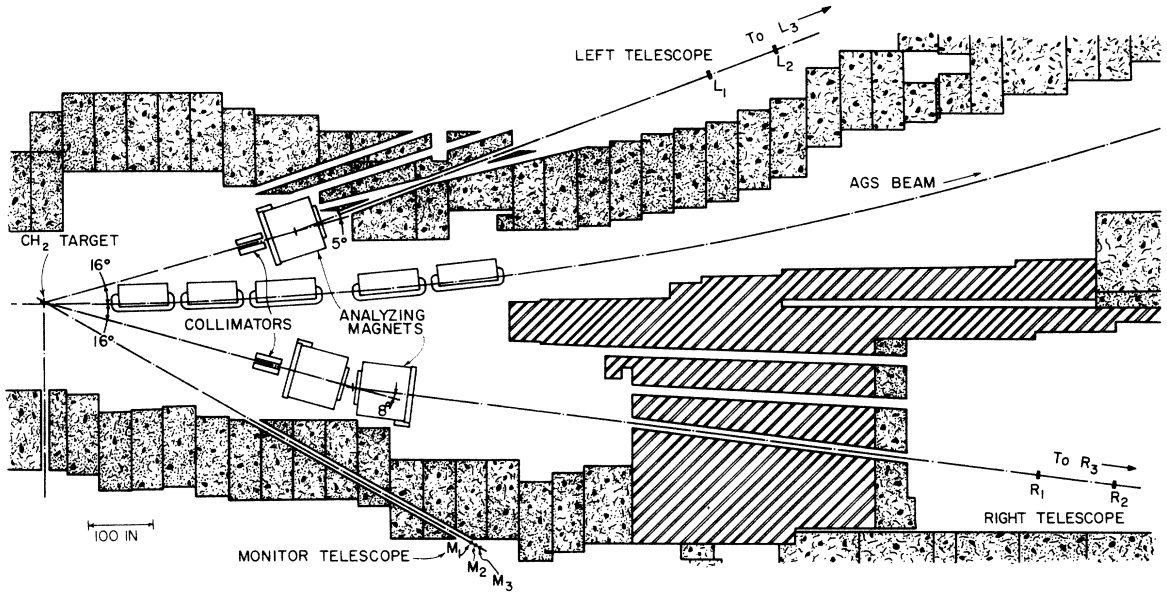

FIG. 1. Experimental layout for the highest momentum transfer experiment. Internal beam momentum $P_0 = 21.9$ BeV/c and squared four-momentum transfer $-t = 19.6$ (BeV/c)^2.

angular distributions are similar and appear to be almost constant over ~40% of the solid angle ($\theta_{c.m.} = 65°$ to 90°).

The experimental layout for the highest momentum transfer experiment is shown in Fig. 1. The internal proton beam of the AGS is scattered by hydrogen in a polyethylene target. The scattered and recoil protons leaving the target pass through collimators placed at the calculated angles corresponding to a particular beam energy. Then the protons pass through deflection magnets tuned to select the calculated momenta. Following these magnets are the left and right counter telescopes which identify an elastic p-p scattering by a left-right coincidence. The only significant background using this technique was found to be due to accidental coincidences between the two telescopes. Coincidences were displayed using a time-to-pulse-height converter feeding into a pulse-height analyzer. Full width at half-maximum of the peak observed in the pulse-height analyzer was 2×10^{-9} sec.

Instantaneous counting rates were reduced by spilling the beam slowly onto the target (usually ~10^{11} protons for about 0.2 sec). In order to achieve a uniform spill of beam over this time interval, it was necessary to use fairly thin targets. Problems of melting and hydrogen depletion were overcome by using a 1-mm thick polyethylene wheel which rotated several degrees with each flip of the target.[2]

The laboratory solid angles were defined by counter size in one of the two telescopes and were typically on the order of 10^{-4} steradian. The solid angle subtended by the other telescope was made larger to allow for uncertainties in beam energy, magnet current settings, and multiple scattering in target and air.

The contribution to the coincidences due to the presence of carbon in the CH_2 target was measured using a pure carbon target and found to be less than 2% of the effect observed with CH_2 target. This is consistent with an estimate of the quasielastic scattering of protons on protons in the carbon nucleus by taking into account the smearing out of the angular correlation due to the Fermi motion. Hence the coincidences observed with polyethylene targets are practically all due to elastic scattering by hydrogen.

Any coincidences due to inelastic interactions with the hydrogen should occur with the carbon as well. Since pion distributions from carbon and hydrogen are similar, we would expect that inelastic background must also be less than ~2%. This has been confirmed by several other tests. Whenever the beam energy or magnet currents were changed by several percent from their calculated values, the coincidences disappeared. When the counter sizes on both telescopes were reduced, the coincidence rate decreased proportionally to the first power of the solid angle of the defining telescope rather than the product of

the solid angles of both telescopes. Of course, each event would have a small inelasticity due to the production of soft photons. Up to a few percent of our p-p scatters might be lost because of this. Due to the lack of an adequate theory, we have made no radiative correction.

In order to obtain an absolute cross section, the monitor telescope was calibrated in terms of the number of beam protons passing through the target. This was done by counting the 0.48-MeV gamma ray following the decay of the Be^7 spallation product from carbon. In our calculations we have used the value 9.5 mb for Be^7 spallation cross section,[3] and 10.32% for the branching ratio to the 0.48-MeV gamma ray.[4]

The cross section results are given in Table I. The statistical errors were usually less than ±10% and never more than ±16%. We estimate a systematic error due to uncertainties in alignment and geometry of +10%, -0%. The error of the Be^7 cross section is ±10%. Other systematic errors due to uncertainties of our estimate of absorption in the counters and determinations of the Be^7 gamma-ray count amount to an estimated ±10%. Table I contains the combined systematic and statistical errors, and also contains values of X as well as $d\sigma/d\omega$, where

$$X = \frac{(d\sigma/d\omega)_{\text{c.m.}}}{(d\sigma/d\omega)_0}$$

and

$$(d\sigma/d\omega)_0 = (k\sigma_T/4\pi)^2.$$

The latter equation uses the optical theorem to obtain the zero-degree differential cross section. We use 40 mb for σ_T, the total p-p cross section.

The values of X are plotted vs $-t$ in Fig. 2. We see that at higher momentum transfer the points are not decreasing as fast with $-t$ as are the points at lower momentum transfer. In addition to this dependence on momentum transfer, there is also a dependence on energy which becomes more dominant at high momentum transfers. For example at $-t = 10$ (BeV/c)^2, X changes by more than a factor of 400 when P_0 changes from 11 to 29 BeV/c.

We have indicated by the three dashed curves the approximate behavior of X as a function of t for incoming protons of fixed momentum. The end points of these curves correspond to $t_{\max}$

Table I. The eighteen p-p elastic cross sections measured in this experiment.

$-t$ (BeV/c)^2	P_0 (BeV/c)	$\theta_{\text{c.m.}}$ (deg)	$(d\sigma/d\omega)_{\text{c.m.}}$ (cm^2/sr)	X	Percent error in $d\sigma/d\omega$ and X (%)
2.28[a]	13.0[b]	37.0[c]	3.06×10^{-30}	2.06×10^{-5}	+25,-20
3.16	16.1	40.8	5.12×10^{-31}	2.74×10^{-6}	+25,-20
4.30	13.1	51.5	1.30×10^{-31}	8.77×10^{-7}	+25,-20
4.30	18.1	42.8	7.43×10^{-33}	3.51×10^{-7}	+25,-20
6.00	11.1	68.3	4.02×10^{-32}	3.22×10^{-7}	+25,-20
6.00	15.7	55.4	1.29×10^{-32}	7.04×10^{-8}	+25,-20
6.00	21.7	46.2	5.98×10^{-33}	2.35×10^{-8}	+25,-20
7.80	12.9	72.1	9.83×10^{-33}	6.68×10^{-8}	+25,-20
7.80	18.2	58.8	2.52×10^{-33}	1.18×10^{-8}	+25,-20
7.80	25.0	49.1	9.78×10^{-34}	3.31×10^{-9}	+25,-20
9.90	11.4	90.0	2.24×10^{-32}	1.74×10^{-7}	+25,-20
10.00	14.2	78.4	5.10×10^{-33}	3.11×10^{-8}	+25,-20
10.00	20.9	62.1	4.84×10^{-34}	1.97×10^{-9}	+25,-20
10.00	28.7	52.0	1.47×10^{-34}	4.30×10^{-10}	+30,-25
11.12	30.7	53.7	4.47×10^{-35}	1.23×10^{-10}	+30,-25
12.01	16.0	81.4	1.54×10^{-33}	8.30×10^{-9}	+25,-20
14.50	18.0	86.0	3.65×10^{-34}	1.74×10^{-9}	+25,-20
19.65	21.9	90.0	5.15×10^{-35}	2.00×10^{-10}	+30,-25

[a] All squared four-momentum transfers, t, have an error of ±1%.
[b] All internal beam momenta, P_0, have an error of ±1%.
[c] All center-of-mass scattering angles have an error of ±0.2°.

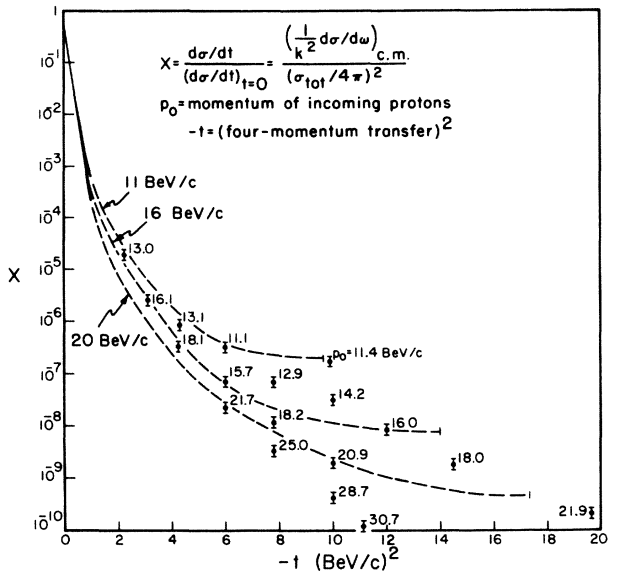

FIG. 2. Elastic differential cross section, normalized to the forward scattering cross section, as a function of the squared four-momentum transfer $-t$. The heavy lines from $-t=0$ to 1 (BeV/c)^2 are from the work of K. J. Foley, S. J. Lindenbaum, W. A. Love, S. Ozaki, J. J. Russell, and L. C. L. Yuan, Phys. Rev. Letters 10, 376 (1963). Dashed lines describe the behavior of X at fixed beam momenta of 11, 16, and 20 BeV/c; each line ends at t_{max} which corresponds to $\theta_{c.m.}=90°$.

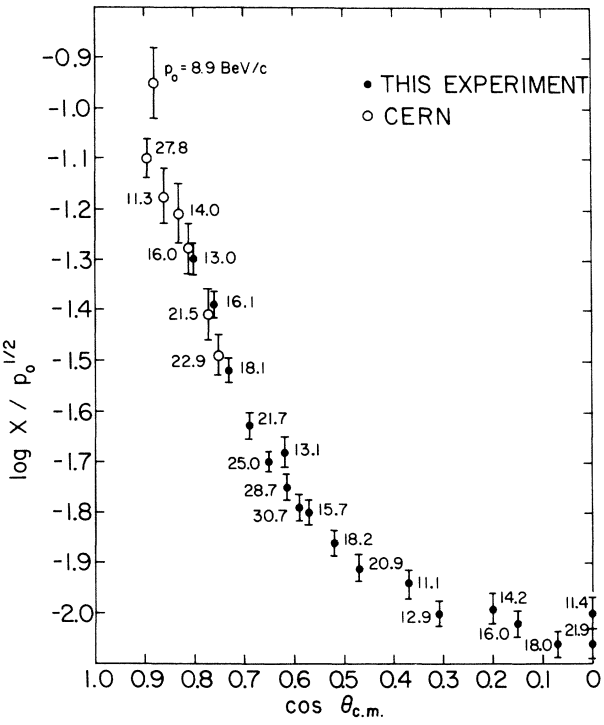

FIG. 3. Shape of the angular distribution obtained by plotting $(\log_{10}X)/P_0^{1/2}$ vs $\cos\theta$. The CERN points are from reference 1.

which occurs when $\theta_{c.m.}$ is 90°. Since $t/t_{max} = 1 - \cos\theta_{c.m.}$, these curves show directly the shape of the angular distributions. Although it is expected that the angular distribution curve for the scattering of two identical particles must have zero slope at 90°, it is surprising to see these curves suddenly flatten out well before reaching the 90° region after a steep descent of many orders of magnitude. The three dashed curves, if plotted on the same horizontal scale, appear similar in shape but with heights ($\log X$) that appear to be proportional to $P_0^{-1/2}$. This relationship can be conveniently displayed by plotting $(\log X)/P_0^{1/2}$ vs $\cos\theta$ as is done in Fig. 3. In addition to our points, we have also plotted the cross sections measured at CERN[1] which are above 10 BeV and have $\cos\theta$ less than 0.9. It is clear that all these points are statistically consistent with one common shape of angular distribution. Lower energy results from Berkeley[5] do not agree so closely. A simple expression which approximately fits the points in Fig. 3 is

$$(\log_{10}X)/P_0^{1/2} = -2(1 - 0.9\cos^4\theta_{c.m.}),$$

where P_0 is in BeV/c.

We wish to thank Mr. Bruce Ulrich for assisting in the later stages of this experiment and Dr. J. Hudis for useful discussions and the Be[7] analysis of our many targets. We are grateful to Dr. R. Sugarman of Chronetics, Inc., for helpful advice concerning the electronics. We are most indebted to the AGS staff for their invaluable cooperation and help with various special problems of direct concern to this experiment such as the rotating target and the fine-cut control of the flat top (beam energy adjustable in 50-MeV steps).

---

*Research supported by the U. S. Atomic Energy Commission and a research grant from the National Science Foundation.

†Present address: CERN, Geneva, Switzerland.

[1]W. F. Baker, E. W. Jenkins, A. L. Read, G. Cocconi, V. T. Cocconi, and J. Orear, Phys. Rev. Letters 9, 221 (1962); A. N. Diddens, E. Lillethun, G. Manning, A. E. Taylor, T. G. Walker, and A. M. Wetherell, Phys. Rev. Letters 9, 111 (1962).

[2]The target mechanism was designed by C. R. Flatau (to be published).

[3]J. B. Cummings, J. Hudis, A. M. Poskanzer, and S. Kaufman, Phys. Rev. 128, 2392 (1962).

[4]J. G. V. Taylor and J. S. Merrit, Can. J. Phys. 40, 926 (1962).

[5]B. Cork, W. A. Wenzel, and C. W. Causey, Jr., Phys. Rev. 107, 859 (1957).

ANTIPROTON AND KAON ELASTIC SCATTERING AT HIGH ENERGIES*

K. J. Foley, S. J. Lindenbaum, W. A. Love, S. Ozaki, J. J. Russell, and L. C. L. Yuan
Brookhaven National Laboratory, Upton, New York
(Received 7 November 1963)

This Letter reports measurements of differential elastic cross sections for $\bar{p}$-p scattering at 7.2, 8.9, 10.0, and 12.0 BeV/c, for K^+-p at 6.8, 9.8, 12.8, and 14.8 BeV/c, and for K^--p at 7.2 and 9.0 BeV/c. For $\bar{p}$-p the range of four-momentum transfer squared, t, covered is $0.03 < -t < 0.6$ $(\text{BeV}/c)^2$ and for $K^{\pm}$-p, $0.03 < -t < 1.1$ $(\text{BeV}/c)^2$. There is some evidence that the $\bar{p}$-p system does not exhibit the "Regge-pole" shrinkage observed in the p-p system, while the behavior of the K^+-p system is consistent with that of p-p. Data on K^--p are not sufficient to draw shrinkage conclusions.

All measurements were made using the hodoscopes and data handling systems employed to measure $\pi^{\pm}$ and p scattering.[1] They include cross sections at small angles, obtained by measuring the momentum of the scattered particle to establish elasticity, and cross sections for $|t| > 0.25$ $(\text{BeV}/c)^2$ measured by observing the angular correlation of scattered and recoil particles. These have been combined using the relative normalization factor deduced previously for $\pi^{\pm}$ and p scattering. Corrections were applied to the two sets of data to allow for $K^{\pm}$ decay; these corrections were calculable to an accuracy of a few percent and introduce, therefore, no appreciable additional error.

The resulting differential cross sections with their appropriate t values, as well as values of

Table I. The experimental cross sections. Under each momentum are given the total elastic cross section, the ratio of the elastic to the total cross section, the result of extrapolating the measured values of $d\sigma/dt$ to $t = 0$, and a table of the t values and cross sections. The results of the magnetic analysis system are marked with an asterisk. Values of $d\sigma/dt$ are given in mb/$(\text{BeV}/c)^2$, and the units of t are $(\text{BeV}/c)^2$. In addition to the errors given, there is an over-all systematic scale uncertainty of ±5% for $\bar{p}$-p, ±7% for $K^{\pm}$-p, and a relative normalization uncertainty of ±3% between the two sets of data.

	$\bar{p}$-p			
P	7.2 BeV/c	8.9 BeV/c	10.0 BeV/c	12.0 BeV/c
σ_{el}	13.79 ± 1.00 mb	13.89 ±0.35 mb	14.6 ± 3.3 mb	11.59 ±0.41 mb
σ_{el}/σ_t	0.226 ± 0.017	0.238 ±0.009	0.257 ± 0.058	0.213 ±0.010
$d\sigma/dt(0)$	181 ±16	178 ±5.1	173 ±47	147 ±6.4
	$-t$ $d\sigma/dt$	$-t$ $d\sigma/dt$	$-t$ $d\sigma/dt$	$-t$ $d\sigma/dt$
	*0.026 131 ±20	*0.024 127.0 ±6.3	*0.030 122 ±31	*0.043 80.9 ±4.2
	*0.037 84 ±18	*0.038 114.0 ±5.2	*0.049 75 ±23	*0.070 62.1 ±3.3
	*0.052 113 ±18	*0.058 83.9 ±3.9	*0.074 82 ±18	*0.105 38.1 ±2.3
	*0.070 72 ±14	*0.082 57.0 ±3.1	*0.105 56 ±15	*0.149 24.9 ±1.8
	*0.089 39.0 ±11.1	*0.110 43.9 ±2.8	*0.140 27 ±12	*0.198 12.2 ±1.3
	*0.109 47.9 ± 8.2	*0.138 32.6 ±2.2	*0.176 19 ±10	*0.249 7.15 ±0.95
	0.272 4.95 ± 0.44	*0.172 20.5 ±1.6		0.268 4.09 ±0.44
	0.349 2.01 ± 0.25	0.264 5.23 ±0.42		0.343 1.96 ±0.27
	0.434 0.42 ± 0.12	0.338 2.48 ±0.24		0.428 0.583 ±0.132
	0.524 0.24 ± 0.09	0.422 0.77 ±0.13		0.517 0.190 ±0.091
		0.508 0.282 ±0.077		
		0.602 0.091 ±0.045		

(Continued on p. 504.)